**ARTICLE**

# Optimized Three-Dimensional Cardiovascular Magnetic Resonance Whole Heart Imaging Utilizing Non-Selective Excitation and Compressed Sensing in Children and Adults with Congenital Heart Disease

**Ingo Paetsch[1],[*], Roman Gebauer[2], Christian Paech[2], Frank-Thomas Riede[2], Sabrina Oebel[1], Andreas Bollmann[1], Christian Stehning[3], Jouke Smink[4], Ingo Daehnert[2] and Cosima Jahnke[1]**

[1]Department of Electrophysiology, Heart Center Leipzig at University of Leipzig, Leipzig, Germany

[2]Department of Pediatric Cardiology, Heart Center Leipzig at University of Leipzig, Leipzig, Germany

[3]Philips Research Laboratories, Hamburg, Germany

[4]Philips Medical Systems, Best, The Netherlands

[*]Corresponding Author: Ingo Paetsch. Email: ingo.paetsch@icloud.com

## ABSTRACT

**Background:** In congenital heart disease (CHD) patients, detailed three-dimensional anatomy depiction plays a pivotal role for diagnosis and therapeutical decision making. Hence, the present study investigated the applicability of an advanced cardiovascular magnetic resonance (CMR) whole heart imaging approach utilizing nonselective excitation and compressed sensing for anatomical assessment and interventional guidance of CHD patients in comparison to conventional dynamic CMR angiography. **Methods:** 86 consecutive pediatric patients and adults with congenital heart disease (age, 1 to 74 years; mean, 35 years) underwent CMR imaging including a free-breathing, ECG-triggered 3D nonselective SSFP whole heart acquisition using compressed SENSE (nsWHcs). Anatomical assessability and signal intensity ratio (SIR) measurements were compared with conventional dynamic 3D-/4D-MR angiography. **Results:** The most frequent diagnoses were partial anomalous pulmonary venous drainage (17/86, 20%), transposition of the great arteries (15/86, 17%), tetralogy of Fallot (12/86, 14%), and a single ventricle (7/86, 8%). Image quality of nsWHcs was rated as excellent/good in 98% of patients. nsWHcs resulted in a reliable depiction of all large thoracic vessels (anatomic assessability, 99%–100%) and the proximal segments of coronary arteries and coronary sinus (>90%). nsWHcs achieved a homogenously distributed SIR in all cardiac cavities and thoracic vessels without a significant difference between pulmonary and systemic circulation (10.9 ± 3.5 and 10.6 ± 3.4; $p = 0.15$), while 3D angiography showed significantly increased SIR for targeted *vs.* non-targeted circulation (PA-angiography, 15.2 ± 8.1 *vs.* 5.8 ± 3.6, $p < 0.001$; PV-angiography, 7.0 ± 3.9 *vs.* 17.3 ± 6.8, $p < 0.001$). **Conclusions:** The proposed nsWHcs imaging approach provided a consistently high image quality and a homogeneous signal intensity distribution within the pulmonary and systemic circulation in pediatric patients and adults with a wide spectrum of congenital heart diseases. nsWHcs enabled detailed anatomical assessment and three-dimensional reconstruction of all cardiac cavities and large thoracic vessels and can be regarded particularly useful for preprocedural planning and interventional guidance in CHD patients.

## 1 Introduction

Cardiovascular magnetic resonance (CMR) has become a diagnostic cornerstone in children and adults with congenital heart disease (CHD) [1,2]. Current guidelines for the management of CHD patients acknowledge CMR imaging as the accepted reference standard for ventricular volume and function assessment, blood flow measurements and myocardial tissue characterization [3–5].

However, besides the hemodynamic and structural evaluation, CMR offers the additional advantage of a detailed three-dimensional depiction of complex congenital heart defects. Accurate anatomical visualization represents a prerequisite for stratification and therapeutical decision making with three-dimensional reconstruction of the targeted cardiac cavities and vessels being an integral part of preprocedural planning and interventional guidance especially during electrophysiology procedures [3]. However, a universal CMR imaging strategy covering the small structures in infants or small children as well as the wide variability of cardiac and vessel anatomy before and after multiple surgical interventions in CHD patients remains challenging.

Currently, contrast-enhanced CMR angiography is usually recommended for three-dimensional visualization of large thoracic vessels and can be rapidly acquired during a single breath-hold. Yet, dynamic CMR angiography relies on adequate timing of image acquisition depending on the clinical question, and three-dimensional visualization is mostly restricted to the targeted vessel territories only [2]. Alternatively, ECG-triggered, navigator-gated 3D steady-state free precession (SSFP) imaging has been utilized with the advantage of depicting all cardiac and extra-cardiac structures [2]. So far, free-breathing 3D SSFP imaging has been established mainly for the depiction of the coronary arteries with a routine application being limited to the evaluation of coronary artery anomalies [2,6]. The limited first-line usage of 3D SSFP whole heart imaging in CHD patients may currently be attributed to long scan durations, low spatial resolution, laborious scan planning, and degraded image quality due to inhomogeneous endoluminal signal intensity distribution. However, recent technical advances such as the invention of compressed SENSE for cardiac imaging or nonselective radiofrequency excitation for SSFP imaging could help to overcome these obstacles [7,8]. Compressed SENSE is expected to considerably speed up CMR imaging while maintaining high image quality. The use of a nonselective radiofrequency excitation has the potential to reduce signal loss and image artifacts of SSFP sequences [9,10].

Hence, the present study investigated the applicability of free-breathing, 3D nonselective SSFP imaging using compressed SENSE for anatomical characterization and interventional guidance of pediatric patients and adults with congenital heart disease in comparison to conventional dynamic CMR angiography.

## 2 Methods

### 2.1 Patient Population

Children and adults with congenital heart disease referred for interventional or surgical treatment were consecutively included. All CMR exams were clinically indicated by the treating pediatric cardiologist and the CMR protocol was individually tailored to the clinical question. The study was conducted in accordance with the local institutional review board and the standards of the University of Leipzig ethics committee; written informed consent was obtained from all patients or parents, respectively. CMR examinations of patients with implanted pacemakers or defibrillators were not considered.

### 2.2 CMR Imaging Protocol

CMR imaging was done using a 1.5 Tesla MR scanner (Philips Ingenia, Best, The Netherlands) equipped with a 28-element array coil with full in-coil signal digitalization and optical transmission. Patients were continuously monitored throughout the entire procedure by an experienced cardiologist. Physiologic monitoring consisted of a vector-surface ECG, peripheral pulse oximetry, assessment of respiratory motion pattern, and non-invasive blood pressure measurements; throughout the entire procedure visual and voice contact with the patient was maintained. The CMR protocol was individually tailored to patient's size, age and the specific clinical question. CMR imaging data were continuously evaluated during the imaging procedure by a certified cardiological CMR imaging expert and imaging parameters were directly adapted if necessary. Young children (typically less than age 8 to 9 years) usually required a deep sedation using propofol and midazolam while spontaneous breathing was maintained. Older children and adults were mostly cooperative and followed the breath-hold commands; for anxiolysis (e.g., in case of a claustrophobic reaction), diazepam was administered intravenously if desired.

Cardiac cine imaging, flow measurements and an anatomical three-dimensional SSFP scan covering the entire thorax represented the crucial components and were, thus, an integral part of all CMR examinations. Myocardial tissue characterization (e.g., T1-/T2-weighted imaging, late gadolinium enhancement imaging), myocardial perfusion imaging or contrast-enhanced MR angiography were acquired in addition if necessary.

### 2.2.1 Cardiac Cine Imaging

Cine images adhered strongly to current recommendations (SSFP sequence; measured in-plane spatial resolution, 1.2–1.5 mm; slice thickness, 6–8 mm; temporal resolution, >30 phases per cardiac cycle) and were usually acquired during repetitive expiratory breath-holding [11]. All standard cardiac geometries were covered (i.e., multiple, gap-less short axis views and a 4-, 3-, and 2-chamber view); additional geometries were added when needed (e.g., aortic valve, right-ventricular outflow tract). In sedated patients, a free-breathing approach with multiple signal averages (NSA) was applied in order to minimize the effect of respiratory variation [11].

End-diastolic and end-systolic volumes of the systemic and the subpulmonary ventricle were measured according to standard definitions and indexed to body surface area [12,13]. Ejection fraction of the systemic and subpulmonary ventricles were calculated accordingly.

### 2.2.2 Phase-Contrast Flow Measurements

Two-dimensional phase-contrast flow measurements were performed in the ascending aorta and the main pulmonary artery with the imaging plane 10 mm above the aortic and pulmonary valve, respectively [11]. The imaging plane was carefully placed perpendicular to the flow direction (in-plane spatial resolution, 1.2–1.4 mm; slice thickness, 8–10 mm; temporal resolution, >30 phases per cardiac cycle); velocity encoding was routinely set to 150 cm/s but individually adapted if necessary. Additional flow measurements (e.g., separate measurements of left and right pulmonary artery, aortic isthmus) were added when needed. In sedated patients, a free-breathing approach with multiple signal averages (NSA) was applied [11].

Semi-automatic vessel border detection was used to measure antegrade and retrograde volumes; regurgitant fraction, cardiac output and pulmonary-systemic flow ratio (Qp/Qs) were calculated accordingly [12].

### 2.2.3 3D Whole Heart Imaging: Nonselective Balanced SSFP Using Compressed SENSE (nsWHcs)

A free-breathing, ECG triggered three-dimensional bright-blood balanced SSFP sequence was employed for detailed anatomical assessment of cardiac cavities and large thoracic vessels. Navigator gating with continuous drift correction was used for respiratory motion compensation and patients were

allowed to breath freely during image acquisition. A T2-preparation prepulse and large flip angle ($\alpha = 90°$) were applied to increase the contrast between arterial blood and surrounding tissues. A hard (nonselective) RF block excitation pulse was used without slice selection gradients for short repetition and echo times (TR/TE, 2.3/1.1 ms), thereby reducing susceptibility to banding or flow artifacts, and thus, yielding optimized signal homogeneity. Compressed SENSE was employed in both phase encoding directions (total acceleration factor 5.0) to minimize scan time (nominal scan duration, <120 s). Image acquisition was done in coronal slice orientation with a large field-of-view covering the entire thorax. A high isotropic spatial resolution guaranteed immaculate three-dimensional reconstruction and segmentation of cardiac cavities/great thoracic vessels (reconstructed spatial resolution, 0.7 mm × 0.7 mm × 0.7 mm – 0.9 mm × 0.9 mm × 0.9 mm); acquisition duration per heartbeat was individually adapted to the diastolic cardiac rest period and mainly depended on heart rate (acquisition duration, 50–180 ms).

### 2.2.4 CMR Angiography

Contrast-enhanced, dynamic 3D MR angiography targeted either the pulmonary or the systemic circulation. If the preferred target circulation could not be specified in advance, 4D MR angiography was applied alternatively. In general, CMR angiography was conducted during inspiratory breath-holding without ECG triggering during first-pass of the contrast agent in the target region (coronal slice orientation; full coverage of the great thoracic vessels and cardiac cavities). Dynamic 3D angiography utilized a spoiled gradient echo sequence with isotropic spatial resolution (1.2 mm × 1.2 mm × 1.2 mm; number of slices, 90–120; TR/TE/flip angle, 2.6/0.8 ms/25°; breath-hold duration, 10–12 s). Real-time bolus tracking was used for accurate timing during contrast agent bolus injection via a superficial vein of the upper limbs (Gadoteric acid; 0.1 mmol/kg bodyweight; injection rate, 4.0 ml/s) [14].

Dynamic 4D angiography utilized a spoiled gradient echo sequence with 6–8 dynamics (temporal resolution, 2.6 s; spatial resolution, 1.0 mm × 1.0 mm × 1.0 mm; number of slices, 100–120; TR/TE/flip angle, 4.0/1.1 ms/25°). Image data acquisition was started 4–6 s after contrast agent bolus injection (Gadoteric acid; 0.1 mmol/kg bodyweight; injection rate, 2.0 ml/s).

### 2.3 Pre- vs. Postcontrast nsWHcs

A pre-study was conducted to facilitate direct comparison of pre- *vs.* postcontrast nsWHcs with regard to image quality and intraluminal signal homogeneity: a separate study group comprising of twelve adults without congenital heart disease underwent clinically indicated CMR imaging prior to an electrophysiological intervention with nsWHcs imaging carried out twice using the identical scan parameters: first, nsWHcs was acquired prior to contrast agent application and subsequently, the identical scan was repeated about one to two minutes after contrast agent application ("equilibrium phase") during the waiting period for late-gadolinium enhancement imaging. All patients gave written informed consent.

### 2.4 CMR Image Analysis

Image analysis of nsWHcs and angiographic scans was carried out by a certified CMR imaging cardiologist using a dedicated CMR software analysis tool (IntelliSpace Portal 11.1, Philips, Best, The Netherlands). Overall image quality of nsWHcs scans was graded visually with regard to signal homogeneity and vessel sharpness using a four-point scale (excellent, good, moderate, non-diagnostic). Anatomical evaluation of the great thoracic veins (inferior and superior vena cava/innominate vein, pulmonary veins) and arteries (pulmonary artery, thoracic aorta, aortic arch branches) was performed; endovascular compartments were considered assessable if anatomy depiction including anatomical variations and diameter measurements could be carried out with a high level of confidence. Visibility of the ostium and proximal segments (at least 2 cm) of the coronary arteries (left main/left anterior descending, left circumflex, and right coronary artery) and the coronary sinus were evaluated. In all patients, volume-rendering reconstruction was performed, and surface mesh models of the required

cardiac cavities and large thoracic vessels were generated with the exported mesh data used for preprocedural planning and anatomical guidance during subsequent interventional/electrophysiological procedures.

Multiple signal intensity measurements were carried out inside the cardiac cavities and large thoracic vessels on nsWHcs and all angiographic scans. For 4D-angiography, signal intensity measurements were performed in all contrast-enhanced dynamics with the highest signal intensity value of the target region being included in the final analysis. The following measurement locations were predefined for the pulmonary circulation (IVC, SVC, innominate vein, RA, subpulmonary ventricle, main PA, left PA, and right PA) and the systemic circulation (LSPV, LIPV, RSPV, RIPV, LA, systemic ventricle, ascending aorta, aortic arch, and descending aorta), respectively. In patients with a Fontan circulation, signal intensity inside the extra- or intracardiac conduit was measured additionally. Pulmonary parenchyma served as the reference tissue and signal intensity was measured inside a region of interest being carefully placed in the peripheral pulmonary parenchyma while avoiding any cross-sections of segmental pulmonary arteries or veins [15]. Signal intensity ratio (SIR) was calculated by dividing the signal intensity of the target region by the signal intensity of the reference tissue.

### 2.5 Statistical Analysis

All analyses were done using SPSS (version 21, IBM Corporation, Armonk, NY, USA). Continuous variables were given as mean ± standard deviation for normally distributed data; frequencies and percentages were presented for the description of categorical data. Differences between continuous and categorical variables were assessed using Student's $t$-test, ANOVA or Chi-square test as appropriate. All tests were two-tailed; a $p$-value of <0.05 was considered significant. Cohen's kappa was applied to measure agreement between nsWHcs and angiography with regard to the anatomical assessment of PV variants, using the following grading: 0–0.2 (slight), 0.21–0.4 (fair), 0.41–0.6 (moderate), 0.61–0.8 (substantial), and 0.81–1.0 (almost perfect) [16].

## 3 Results

### 3.1 Patient Population

A total of 86 pediatric patients and adults with congenital heart disease were included (43 males; mean age, $35 \pm 20$ years, range: 1–74 years; mean weight, $69 \pm 26$ kg, range 10–172 kg). Mean heart rate during the CMR examination was $77 \pm 21$ bpm (range, 50–190 bpm) and most patients presented with sinus rhythm (77/86, 90%). CMR imaging was performed during sedation with propofol/midazolam in 10 patients (12%; mean age, $8 \pm 7$ years; range, 1–26 years), anxiolytic treatment with diazepam was applied in 7 patients (8%; mean age, $45 \pm 16$ years; range, 18–68 years), while all other patients underwent the CMR examination without any premedication (69/86, 80%; mean age, $38 \pm 19$ years; range, 9–74 years).

The most common leading diagnoses were partial anomalous pulmonary venous drainage (PAPVD; 17/86, 20%), transposition of the great arteries (TGA; 15/86, 17%), tetralogy of Fallot (TOF; 12/86, 14%), and a single ventricle (7/86, 8%). Other diagnoses (35/86, 41%) included congenital heart valve diseases (n = 11), Ebstein anomaly (n = 5), ventricular septal defect (n = 3), Wolff-Parkinson-White (WPW) syndrome (n = 3), atrial septal defect (n = 2), cardiomyopathy (n = 2), double-chambered right ventricle (n = 1), coarctation of the aorta (n = 1), patent ductus arteriosus (PDA, n = 1), aortopulmonary window (n = 1), Bland-White-Garland syndrome (n = 1), coronary artery fistula (n = 1), permanent junctional reciprocating tachycardia (PJRT, n = 1), catecholaminergic polymorphic ventricular tachycardia (CPVT, n = 1), and idiopathic ventricular tachycardia (n = 1). The morphological right ventricle served as the systemic ventricle in 19/86 (22%) of patients.

The majority of patients had already received surgical treatment (52/86, 60%). An atrial septal defect was still present in 7 patients (8%) and had already been repaired surgically or interventionally in 20/86 (23%) or 5/86 (6%), respectively. A ventricular septal defect was still present in 7 patients (8%) and had

been repaired surgically or interventionally in 20/86 (23%) or 1/86 (1%), respectively. Pulmonary, tricuspid, aortic, and mitral valve replacement/surgical reconstruction was previously done in 9/86 (10%), 5/86 (6%), 1/86 (1%) and 2/86 (2%) patients, respectively. Prior PA stenting and coiling of major aortopulmonary collateral arteries has been done in 6/86 (7%) and 3/86 (3%) patients, respectively. Detailed results of CMR data analysis are given in Table 1.

**Table 1:** CMR imaging parameters of all 86 patients

|  | Mean ± SD | Range |
| --- | --- | --- |
| sysVentricle-EDV, ml | 163 ± 77 | 48–491 |
| sysVentricle-EDVI, ml/m$^2$ | 94 ± 38 | 47–256 |
| sysVentricle-EF, % | 52 ± 12 | 13–69 |
| subpulmVentricle-EDV, ml | 162 ± 83 | 33–589 |
| subpulmVentricle-EDVI, ml/m$^2$ | 90 ± 36 | 35–244 |
| subpulmVentricle-EF, % | 57 ± 12 | 13–77 |
| Cardiac output, l/min | 4.8 ± 1.5 | 1.2–9.8 |
| Qp/Qs | 1.1 ± 0.4 | 0.7–3.2 |
| Aortic regurgitation fraction, % | 6 ± 8 | 0–51 |
| Pulmonary regurgitation fraction, % | 8 ± 11 | 0–63 |
| Ascending aorta, mm | 29 ± 7 | 14–50 |
| Descending aorta, mm | 18 ± 4 | 9–26 |
| Main pulmonary artery, mm | 25 ± 8 | 10–51 |

Note: EDV indicates end-diastolic volume; EDVI, end-diastolic volume indexed for body surface area; EF, ejection fraction; Qp, pulmonary flow; Qs, systemic flow; SD, standard deviation; subpulmVentricle, subpulmonary ventricle; sysVentricle, systemic ventricle.

### 3.2 Comparison of Pre- vs. Postcontrast nsWHcs

In the separate pre-study group, pre- and postcontrast nsWHcs scans were successfully acquired in all patients (n = 12; 6 male; mean age, 48 ± 18 years; mean weight, 83 ± 19 kg). Mean heart rate during the CMR examination was 74 ± 14 bpm (range, 54–102 bpm) and all patients presented with sinus rhythm. Overall image quality of precontrast nsWHcs was rated excellent 7/12 (58%) or good 5/12 (42%) while postcontrast nsWHcs achieved excellent image quality in all patients (12/12, 100%). SIR measurements within cardiac cavities and thoracic vessels proved an overall tendency towards higher SIR values for postcontrast nsWHcs when compared to precontrast nsWHcs (mean SIR difference, 2.1; $p$ = n.s.); the greatest gain with a significant SIR increase was documented for all four pulmonary veins (mean SIR difference, 4.4; $p$ < 0.02) and the coronary sinus (SIR difference, 4.1; $p$ = 0.017). Mean SIR measurements for direct comparison of pre- vs. postcontrast nsWHcs are detailed in Fig. 1.

### 3.3 Nonselective Whole Heart Imaging Using Compressed SENSE (nsWHcs)

Taking into account the results of the pre-study, nsWHcs was predominantly acquired after contrast agent application (83/86 patients; 97%). Mean nominal scan duration of nsWHcs was 95 ± 13 s (range, 55–119 s). nsWHcs delivered an excellent/good image quality in 98% (84/86) of patients (excellent, 73/86 (85%); good, 11/86 (13%); moderate, 2/86 (2%)) while none was considered non-diagnostic. Image quality did not significantly differ between patients with and without sinus rhythm ($p$ = 0.409). Volume-rendering reconstruction was performed successfully in all patients (86/86, 100%).
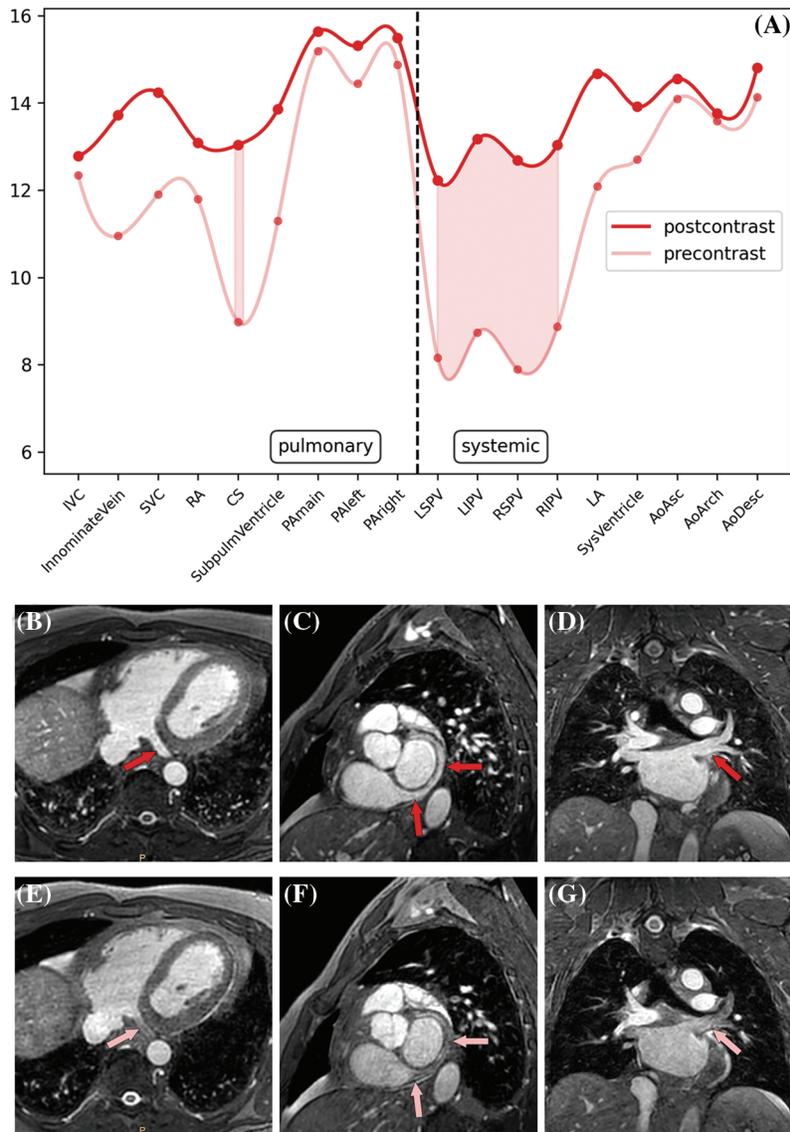
**Figure 1:** Pre- *vs*. postcontrast signal intensity ratios (SIR) of nonselective WholeHeart compressed SENSE (nsWHcs) cardiovascular magnetic resonance imaging. (A) Direct comparison of pre- *vs*. postcontrast SIR measurements depending on vascular/endocavitary anatomy (plot represents third-degree polynomial spline fit of mean SIR values, shaded area indicates maximal SIR gain in respective vascular/endocavitary compartments). (B–D) Postcontrast nsWHcs geometries demonstrating homogeneous intraluminal/ intracavitary bloodpool signal with maximum improvement regarding visibility/demarcation of coronary sinus and pulmonary vein anatomy (red arrows). (E–G) Identical precontrast nsWHcs geometries of coronary sinus and pulmonary vein anatomy (pink arrows)

Note: IVC indicates inferior vena cava; SVC, superior vena cava; RA, right atrium; CS, coronary sinus; SubpulmVentricle, sub-pulmonary ventricle; PA, pulmonary artery; LSPV, left superior pulmonary vein; LIPV, left inferior PV; RSPV, right superior PV; RIPV, right inferior PV; LA, left atrium; SysVentricle, systemic ventricle; Ao, aorta; Asc, ascending; Desc, descending.

Anatomical variants of pulmonary veins, caval veins, and aortic arch branches were assessed with a high level of confidence in 85/86 (99%), 86/86 (100%) and 86/86 (100%) patients, respectively (see Table 2). PV anatomy revealed a left- or right-sided common ostium in 16/86 (19%) or 3/86 (3%) patients, respectively, a common ostium of both inferior PVs in 2 (2%), an accessory right middle PV in 9/86 (11%), and a left-or right-sided PAPVD in 6/86 (7%) or 10/86 (12%) patients, respectively. Caval vein anatomy showed a persistent left superior vena cava in 3/86 patients (3%), an azygos continuation of the inferior vena cava in 3/86 patients (3%), a bidirectional Glenn shunt in 3/86 (3%), and a total cavopulmonary connection (TCPC) in 4/86 (5%). Aortic arch variants included a bovine arch in 8/86 patients (9%), an aberrant right subclavian artery (arteria lusoria) in 4/86 patients (5%), and a direct vertebral artery/right common carotid artery origin from the aortic arch in 2/86 patients (2%). The origin and proximal parts of the coronary arteries and coronary sinus were assessable in >90% of patients (see Table 2); two coronary anomalies were depicted which were both confirmed on invasive coronary angiography.

**Table 2:** Assessability of thoracic endovascular anatomy for nsWHcs and 3D-/4D-angiography

|  | nsWHcs (n = 86) | 3D-Angio PA (n = 18) | 3D-Angio PV (n = 38) | 4D-Angio (n = 8) |
| --- | --- | --- | --- | --- |
| IVC | 86 (100) | 1 (6) | 0 (0) | 6 (75) |
| SVC/innominate vein | 86 (100) | 14 (78) | 2 (5) | 8 (100) |
| PA | 86 (100) | 18 (100) | 17 (45) | 8 (100) |
| PV anatomy | 85 (99) | 4 (22) | 38 (100) | 8 (100) |
| Thoracic aorta | 86 (100) | 3 (17) | 38 (100) | 8 (100) |
| Aortic arch branches | 86 (100) | 3 (17) | 38 (100) | 8 (100) |
| LM-LAD | 84 (98) | 0 (0) | 23 (61) | 1 (13) |
| LCx | 77 (90) | 0 (0) | 8 (21) | 1 (13) |
| RCA | 78 (91) | 0 (0) | 10 (26) | 1 (13) |
| CS | 82 (95) | 6 (33) | 5 (13) | 0 (0) |

Note: CS indicates coronary sinus; IVC, inferior vena cava; LAD, left anterior descending artery; LCx, left circumflex artery; LM, left main; PV, pulmonary vein; RCA, right coronary artery; SVC, superior vena cava.

Mean SIR measurements were not significantly different for children <10 years *vs*. all patients ≥10 years ($11.1 \pm 3.0$ *vs*. $10.7 \pm 3.1$; $p = 0.69$) or for children <40 kg *vs*. all patients ≥40 kg ($11.2 \pm 3.0$ *vs*. $10.7 \pm 3.1$; $p = 0.62$), respectively. In addition, tachycardic heart rate (≥100 bpm) or the presence of sinus rhythm had no significant influence on mean SIR ($10.9 \pm 3.9$ *vs*. $10.7 \pm 3.0$; $p = 0.91$ and $10.7 \pm 3.1$ *vs*. $11.1 \pm 2.5$; $p = 0.72$, respectively).

### 3.4 Comparison of nsWHcs vs. 3D-/4D-Angiography

Dynamic 3D angiography of the pulmonary (PA) or systemic (PV) circulation was performed in 18 (21%) or 38 patients (44%), respectively. 4D angiography was done in 8 patients (9%). Assessability of the great thoracic vessels and the coronary arteries/coronary sinus was summarized in Table 2. With regard to the description of PV anatomy, nsWHcs showed an almost perfect level of agreement with 3D PV-angiography or 4D-angiography (Cohen's kappa, 0.94; $p < 0.001$).

In general, 3D angiography showed the highest SIR within thoracic vessels/cardiac cavities of the target region with a significant drop in the non-targeted circulation (see Table 3). SIR within IVC and intracardiac tunnel or extracardiac conduit were lowest due to intravenous contrast injection via the upper limb (Fig. 2).

For 4D-angiography, differences in SIR measurements were much less pronounced; yet, SIR was significantly higher in the systemic *vs.* pulmonary circulation (Table 3). nsWHcs achieved homogenously distributed SIR values across all thoracic vessels and cardiac cavities without a significant difference between pulmonary and systemic circulation (Table 3).

**Table 3:** SIR measurements for nsWHcs and 3D-/4D-angiography

|  | Pulmonary circulation | Systemic circulation | *p*-value |
| --- | --- | --- | --- |
| 3D PA angiography | $15.2 \pm 8.1$ | $5.8 \pm 3.6$ | <0.001 |
| 3D PV angiography | $7.0 \pm 3.9$ | $17.3 \pm 6.8$ | <0.001 |
| 4D angiography | $9.3 \pm 6.6$ | $11.8 \pm 6.8$ | 0.035 |
| nsWHcs | $10.9 \pm 3.5$ | $10.6 \pm 3.4$ | 0.15 |

Note: nsWHcs indicates nonselective SSFP whole heart imaging using compressed SENSE; PA, pulmonary artery; PV, pulmonary vein; SIR indicates signal intensity ratio.
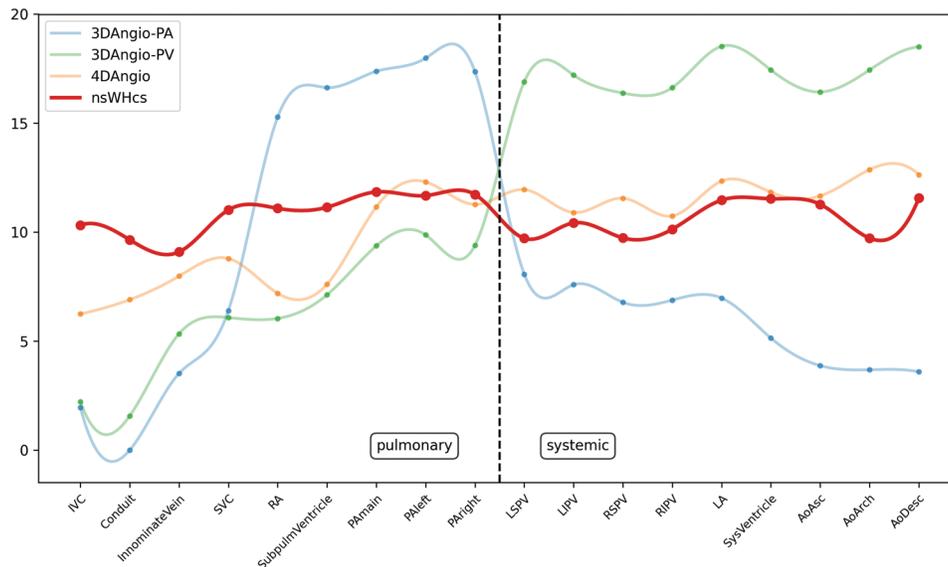


**Figure 2:** Comparative plots of signal intensity ratios (SIR) of contrast-enhanced 3D-/4D-angiography and nonselective WholeHeart compressed SENSE (nsWHcs) cardiovascular magnetic resonance imaging. Plot represents third-degree polynomial spline fit of mean SIR values for dynamic, contrast-enhanced 3D-angiography (bolus-timed to maximum pulmonary arterial or pulmonary venous enhancement), 4D-angiography (temporal resolution of 3D dataset acquisition, 2.6 s) and nsWHcs (i.e., postcontrast equilibrium phase imaging) depending on vascular/endocavitary anatomy

Note: PA indicates pulmonary artery; PV, pulmonary vein; IVC, inferior vena cava; SVC, superior vena cava; RA, right atrium; SubpulmVentricle, subpulmonary ventricle; LSPV, left superior PV; LIPV, left inferior PV; RSPV, right superior PV; RIPV, right inferior PV; LA, left atrium; SysVentricle, systemic ventricle; Ao, aorta; Asc, ascending; Desc, descending.

When comparing 3D PA-angiography with nsWHcs, a significantly higher SIR in the targeted pulmonary circulation was seen while SIR in the systemic circulation was significantly lower (*p* < 0.001 and *p* < 0.001, respectively). Reciprocally, 3D PV angiography achieved a significantly higher SIR in the targeted systemic circulation in comparison to nsWHcs while SIR in the pulmonary circulation was significantly decreased (*p* < 0.001 and *p* < 0.001, respectively). The comparison of 4D-angiography and nsWHcs revealed a significantly higher SIR in the systemic circulation while SIR in the pulmonary

circulation was not significantly different ($p = 0.035$ and $p = 0.201$, respectively). Fig. 2 illustrates all SIR measurements for direct comparison of nsWHcs and 3D-/4D-angiography.

## 4 Discussion

The main findings of the present study were: (1) free-breathing 3D nonselective SSFP imaging with compressed SENSE facilitated full coverage of the entire thorax with a high isotropic spatial resolution in a short nominal scan duration (less than 2 min in all patients) and could be easily integrated into current CMR protocols for preprocedural stratification of children and adults with congenital heart disease, (2) nsWHcs benefitted from prior contrast agent administration especially with regard to the visibility of pulmonary veins and coronary sinus and achieved a good/excellent image quality in nearly all patients (98%), (3) nsWHcs provided uniform signal intensities within all cardiac cavities and large thoracic vessels without a significant difference between pulmonary and systemic circulation, whereas (4) dynamic 3D angiography showed significantly higher SIR within the targeted vessels/cavities but significantly decreased SIR in vessels/cavities of the non-targeted circulation, and (5) nsWHcs achieved an equally high SIR even for IVC and intra- or extracardiac tunnels/conduits in patients with a Fontan circulation substantiating its independence of contrast injection site (unlike dynamic first-pass CMR angiography).

CMR imaging is often requested prior to interventional or surgical treatment when three-dimensional segmentation of the cardiac and vascular cavities is needed for preprocedural planning and peri-procedural guidance [5,17]. Especially in patients with congenital heart disease, detailed anatomical assessment of all cardiac and vascular structures is crucial for therapeutical decision making and interventional assistance (Figs. 3–5, Video S1–S3). At present, contrast-enhanced 3D dynamic MR angiography represents the widely accepted standard for the evaluation of the thoracic vessels in children [2]. However, the timing of image acquisition needs to be designed for the clinical question and depiction of vascular structures is invariably limited to the targeted circulation. The present study corroborated a significant SIR decrease together with a limited anatomical assessability of vascular structures in the non-targeted circulation for conventional 3D MR angiography. When aiming at the anatomical assessment of both, the pulmonary and systemic circulation, 4D MR angiography could be used instead. The most important benefit of the 4D technique relies on the inherent temporal resolution, enabling the assessment of dynamic flow conditions in the observed vascular region. However, the present study data showed that the advantage of a time-resolved MR angiography went at the expense of an overall reduced SIR when compared to 3D angiography which confirmed former study data reporting a decreased image quality of 4D angiography [18]. An additional disadvantage of contrast-enhanced dynamic MR angiography for evaluation of CHD patients relates to the usually ECG untriggered acquisition being designed for extracardiac vessel depiction and, thus, being less suitable for intracardiac morphology evaluation [19].

Implementation of an ECG-triggered, navigator-gated 3D SSFP sequence holds the promise to depict all cardiac, vascular and extravascular structures because of the high signal-to-noise ratio and the intrinsically high contrast. The limited first-line usage of 3D SSFP sequences originates from a few principal disadvantages: a relatively long scan duration (usually approximately 7–10 min), a high susceptibility to artifacts caused by turbulent flow and metallic implants provoking magnetic field inhomogeneities, and a generally impaired image quality in patients with an irregular heartbeat [20]. The use of a nonselective radiofrequency excitation minimizes the susceptibility of SSFP sequences to B0 magnetic field inhomogeneities and out of slice contributions thereby reducing signal loss and image artifacts [10]. On the other hand, nonselective radiofrequency excitation requires a large field-of-view with coverage of the entire thorax resulting in generally prolonged scan durations. Previous studies introduced native 3D nonselective SSFP imaging in a limited number of patients and reported an overall high image quality with sufficient SNR and CNR for the evaluation of arterial and venous thoracic vessels [9,21]. The lowest SNR values were documented for the left atrium while the pulmonary veins were not evaluated [9]. Non-

contrast SSFP acquisitions are generally prone to signal voids or banding artifacts in the left atrium and the PVs, caused by PV off-resonance and/or PV blood flow [22]. The present study demonstrated that postcontrast nsWHcs imaging could overcome the significantly decreased SIR of the pulmonary veins and coronary sinus of precontrast acquisitions.
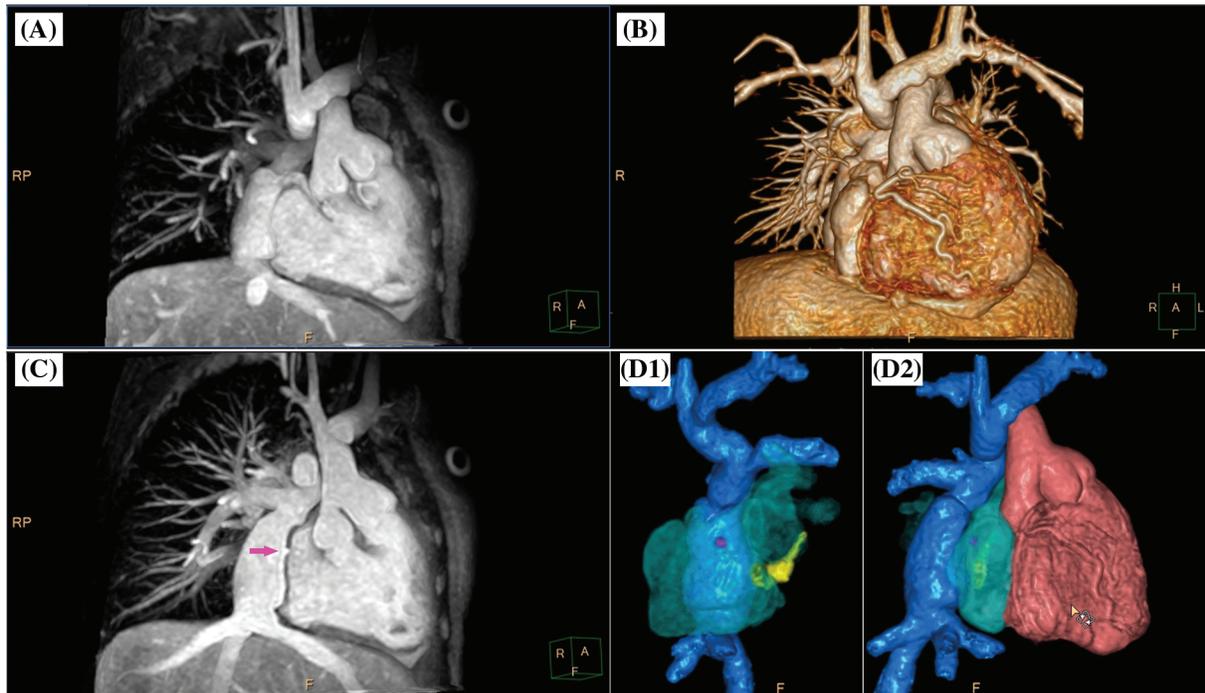


**Figure 3:** Clinical case example I. (A) Volume-intensity projection; (B) volumetric surface rendering; (C) angulated volume-intensity projection for depiction of fenestration site (right anterior oblique angulated view, magenta arrow); D1 and D2, composite volumetric surface rendering of vascular compartments/endoluminal cavities including intracardiac lateral tunnel (blue), fenestration (magenta), atria (transparent green), coronary sinus (yellow) and single ventricle (red). Please refer to video 1 for a fully animated case presentation

The previously provided nonselective SSFP acquisitions were based on a non-isotropic spatial resolution (1.6 mm × 1.6 mm × 3.0 mm) utilizing parallel imaging to shorten scan duration (GRAPPA factor 2.0) with a resultant scan time of 5–10 min [9,10,21]. However, particularly young children may have difficulty with the request to keep absolutely still during this prolonged scan duration. Thus, for pediatric patients and adults with complex congenital heart diseases, the need for a much shorter scan duration together with a high (submillimeter) isotropic spatial resolution could be met by the implementation of compressed sensing for cardiac imaging [7,8]. Compressed sensing methods were recently proposed as a means to considerably accelerate MR data acquisition while maintaining image quality [23,24]. Basically, compressed sensing under-samples data randomly to reduce scan time with the center of k-space being more densely sampled to account for the fact that most of the contrast information arises there [24]. Using compressed SENSE with an acceleration factor of 5.0 in the current study, nominal scan duration was less than 2 min in all patients resulting in a good/excellent image quality in 98% of patients, which underlined its suitability in combination with the large 3D acquisition

volumes associated with the nonselective excitation. A homogeneous SIR distribution of all thoracic vessels and cardiac cavities was seen resulting in a clear depiction of anatomical variants of the large vessels within a wide spectrum of congenital heart diseases (Figs. 3–5, Video S1–S3) [25]. Though contrast injection was done via a superficial vein of the upper limb, postcontrast nsWHcs imaging showed an equally high SIR for the IVC and extracardiac conduits or intracardiac tunnels in patients with a Fontan circulation, thereby proving the independence from the injection site. Moreover, image quality of the proposed nsWHcs scan was not hampered by the presence of numerous metallic implants (e.g., sternal wires, stents, coils, valvular replacements) which is especially important for CHD patients since a majority usually has already undergone previous surgical and/or interventional treatments.
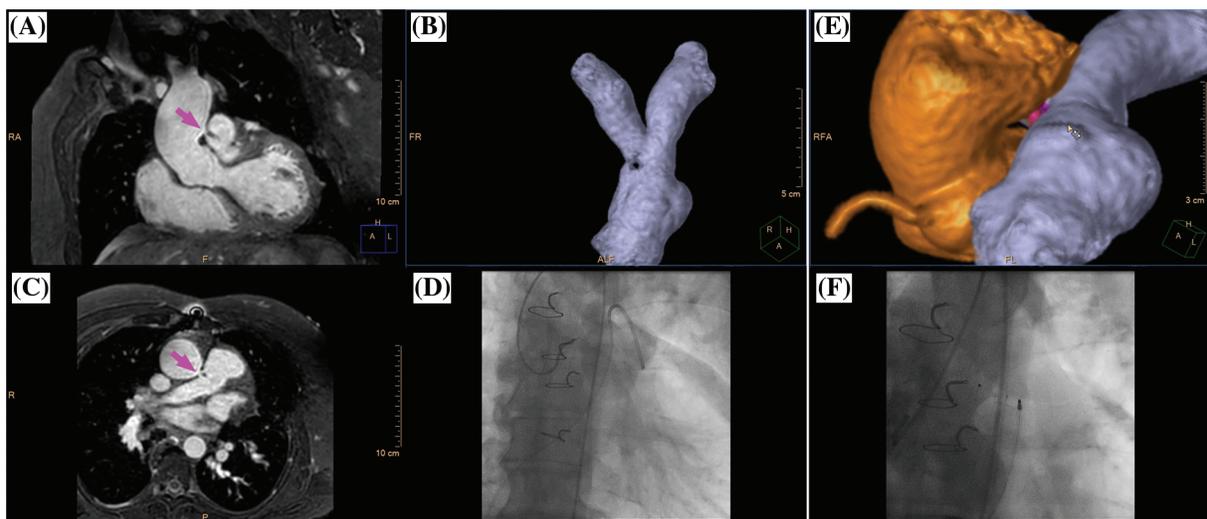


**Figure 4:** Clinical case example II. (A) Multiplanar-reformatted projectional view of nsWHcs for depiction of the aortopulmonary window (coronal geometry, magenta arrow); (B) volumetric-surface rendering of main pulmonary artery bifurcation with clear demarcation of an intraluminal signal loss resulting from jet-related flow disturbances; (C) multiplanar-reformatted projectional view in transversal geometry at the height of the aortopulmonary window (magenta arrow); (D) X-ray fluoroscopy with semi-selective contrast injection of aortopulmonary window and subsequent pulmonary arterial enhancement; (E) volumetric surface rendering of nsWHcs for 3D display of aortic root/ascending aorta (orange), aortopulmonary window (magenta) and main pulmonary artery/pulmonary arterial bifurcation site (blue); (F) X-ray fluoroscopic angiography of thoracic aorta following occluder implantation of aortopulmonary window. Please refer to video 2 for a fully animated case presentation

A previous study on isotropic 3D SSFP imaging in CHD patients found a clear distinction in image quality between infants/younger children and adolescents/adults and concluded that the youngest age at which isotropic 3D SSFP imaging was applicable was 7 years; it was suggested that the higher heart rates of infants/younger children played the most important role for degraded image quality [19]. The present study data invalidated this assumption, since the newly introduced nsWHcs approach resulted in equally high SIR values in both, young children, and patients with high heart rates.
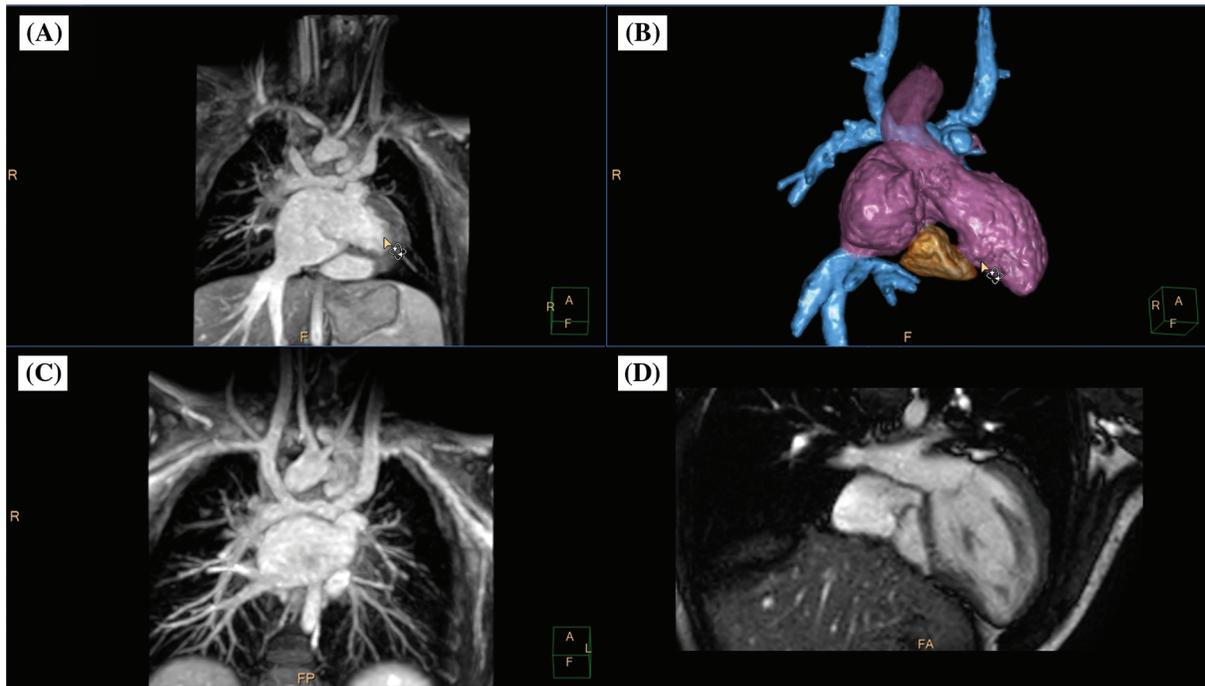
**Figure 5:** Clinical case example III. (A) Animated angulated volume-intensity projection of the nsWHcs dataset; (B) composite volumetric surface rendering of vascular compartments/endoluminal cavities including inferior vena cava and bilateral Glenn anatomy (blue), atria/single ventricle (violet), ascending aorta (transparent violet) and tricuspid annulus/rudimentary right-ventricular cavity (brown); (C) multiplanar-reformatted projectional view of bilateral Glenn anatomy (angulated coronal geometry); (D) cine imaging of an adjusted 4-chamber geometry depicting tricuspid valve/right-ventricular cavity. Please refer to video 3 for a fully animated case presentation

### 4.1 Study Limitations

The current study population was composed of a wide range of congenital heart diseases following various interventional or surgical repairs with resultant biometallic implants. Hence, the study cohort closely reflected the clinical spectrum typically encountered at a highly specialized, tertiary care center and the data as such may only be applicable to a similar clinical scenario.

The CMR protocol was individually tailored to the specific clinical question as well as size, age and the level of cooperation of the respective patient. Consequently, conventional MR angiography has not been performed in all patients or has been targeted to varying vessel territories employing either a 3D- or 4D-acquisition strategy at the discretion of the CMR operator. As a result of these necessary protocol adaptations, a direct comparison between conventional contrast-enhanced CMR angiography and the newly introduced nsWHcs scan could not be rigorously conducted in all study subjects.

### 5 Conclusion

The proposed nsWHcs acquisition could be easily integrated in existing standardized CMR protocols and provided consistently high image quality and a homogeneous signal intensity distribution of the pulmonary and systemic circulation in a study population of children and adults exhibiting a wide spectrum of congenital heart diseases. The nsWHcs imaging approach proved to be independent from contrast injection site, patient age, rhythm and heart rate and allowed for detailed anatomical assessment and three-dimensional reconstruction of cardiac cavities and arterial/venous thoracic vessels including

IVC and extracardiac conduits/intracardiac tunnels in all patients. Thus, nsWHcs can be considered a valuable addition to the diagnostic armamentarium of CMR imaging, particularly with regard to preprocedural planning and interventional guidance in pediatric patients and adults with congenital heart disease.

**Author Contributions:** Study conception and design: I. Paetsch, R. Gebauer, I. Daehnert, C. Jahnke; data collection: I. Paetsch, R. Gebauer, S. Oebel, C. Jahnke; contributions to the sequence design: C. Stehning, J. Smink; analysis and interpretation of results: R. Gebauer, C. Paech, F. T. Riede, A. Bollmann; draft manuscript preparation: I. Paetsch, R. Gebauer, C. Paech, C. Jahnke. All authors reviewed the results and approved the final version of the manuscript.

**Ethics Approval:** Ethics approval was obtained by the local ethics committee of the Faculty of Medicine of the University of Leipzig. For each subject written informed consent was obtained.

**Conflicts of Interest:** Christian Stehning and Jouke Smink are employees at Philips Healthcare. The authors declare that they have no conflicts of interest to report regarding the present study.

## References

1. Dorfman, A. L., Geva, T., Samyn, M. M., Greil, G., Krishnamurthy, R. et al. (2022). SCMR expert consensus statement for cardiovascular magnetic resonance of acquired and non-structural pediatric heart disease. *Journal of Cardiovascular Magnetic Resonance, 24(1),* 44.

2. Valsangiacomo Buechel, E. R., Grosse-Wortmann, L., Fratz, S., Eichhorn, J., Sarikouch, S. et al. (2015). Indications for cardiovascular magnetic resonance in children with congenital and acquired heart disease: An expert consensus paper of the imaging working group of the AEPC and the cardiovascular magnetic resonance section of the EACVI. *European Heart Journal Cardiovascular Imaging, 16(3),* 281–297. https://doi.org/10. 1093/ehjci/jeu129

3. Baumgartner, H., de Backer, J., Babu-Narayan, S. V., Budts, W., Chessa, M. et al. (2021). 2020 ESC guidelines for the management of adult congenital heart disease. *European Heart Journal, 42(6),* 563–645.

4. Fogel, M. A., Anwar, S., Broberg, C., Browne, L., Chung, T. et al. (2022). Society for Cardiovascular Magnetic Resonance/European Society of Cardiovascular Imaging/American Society of Echocardiography/Society for Pediatric Radiology/North American Society for Cardiovascular Imaging Guidelines for the use of cardiovascular magnetic resonance in pediatric congenital and acquired heart disease: Endorsed by the American Heart Association. *Journal of Cardiovascular Magnetic Resonance, 24(1),* 37.

5. Stout, K. K., Daniels, C. J., Aboulhosn, J. A., Bozkurt, B., Broberg, C. S. et al. (2019). 2018 AHA/ACC guideline for the management of adults with congenital heart disease: A report of the American College of Cardiology/ American Heart Association task force on clinical practice guidelines. *Journal of the American College of Cardiology, 73(12),* e81–e192.

6. Hajhosseiny, R., Bustin, A., Munoz, C., Rashid, I., Cruz, G. et al. (2020). Coronary magnetic resonance angiography: Technical innovations leading us to the promised land? *Journal of the American College of Cardiology Cardiovascular Imaging, 13(12),* 2653–2672. https://doi.org/10.1016/j.jcmg.2020.01.006

7. Curione, D., Ciliberti, P., Monti, C. B., Capra, D., Bordonaro, V. et al. (2022). Compressed sensing cardiac cine imaging compared with standard balanced steady-state free precession cine imaging in a pediatric population. *Radiology Cardiothoracic Imaging, 4(2),* e210109. https://doi.org/10.1148/ryct.210109

8. Lin, A. C. W., Strugnell, W., Riley, R., Schmitt, B., Zenge, M. et al. (2017). Higher resolution cine imaging with compressed sensing for accelerated clinical left ventricular evaluation. *Journal of Magnetic Resonance Imaging, 45(6),* 1693–1699. https://doi.org/10.1002/jmri.25525

9. Krishnam, M. S., Tomasian, A., Deshpande, V., Tran, L., Laub, G. et al. (2008). Noncontrast 3D steady-state free-precession magnetic resonance angiography of the whole chest using nonselective radiofrequency excitation over a

large field of view: Comparison with single-phase 3D contrast-enhanced magnetic resonance angiography. *Investigative Radiology, 43(6),* 411–420. https://doi.org/10.1097/RLI.0b013e3181690179

10. Krishnam, M. S., Tomasian, A., Malik, S., Desphande, V., Laub, G. et al. (2010). Image quality and diagnostic accuracy of unenhanced SSFP MR angiography compared with conventional contrast-enhanced MR angiography for the assessment of thoracic aortic diseases. *European Radiology, 20(6),* 1311–1320. https://doi.org/10.1007/s00330-009-1672-3

11. Kramer, C. M., Barkhausen, J., Bucciarelli-Ducci, C., Flamm, S. D., Kim, R. J. et al. (2020). Standardized cardiovascular magnetic resonance imaging (CMR) protocols: 2020 update. *Journal of Cardiovascular Magnetic Resonance, 22(1),* 17. https://doi.org/10.1186/s12968-020-00607-1

12. Schulz-Menger, J., Bluemke, D. A., Bremerich, J., Flamm, S. D., Fogel, M. A. et al. (2020). Standardized image interpretation and post-processing in cardiovascular magnetic resonance—2020 update: Society for Cardiovascular Magnetic Resonance (SCMR): Board of trustees task force on standardized post-processing. *Journal of Cardiovascular Magnetic Resonance, 22(1),* 19. https://doi.org/10.1186/s12968-020-00610-6

13. van der Ven, J. P. G., Sadighy, Z., Valsangiacomo Buechel, E. R., Sarikouch, S., Robbers-Visser, D. et al. (2020). Multicentre reference values for cardiac magnetic resonance imaging derived ventricular size and function for children aged 0–18 years. *European Heart Journal Cardiovascular Imaging, 21(1),* 102–113. https://doi.org/10.1093/ehjci/jez164

14. Lobe, S., Leuthausser, C., Polkow, A., Hilbert, S., Sommer, P. et al. (2021). Optimal timing of contrast-enhanced three-dimensional magnetic resonance left atrial angiography before pulmonary vein ablation. *Cardiology Journal, 28(4),* 558–565. https://doi.org/10.5603/CJ.a2019.0112

15. Oebel, S., Paetsch, I., Stegmann, C., Kircher, S., Sommer, P. et al. (2019). Combined single-session cardiovascular magnetic resonance: Stress perfusion and three-dimensional pulmonary vein angiography for stratification of atrial fibrillation patients with chest pain syndromes prior to catheter ablation. *Europace, 21(12),* 1809–1816. https://doi.org/10.1093/europace/euz248

16. Cohen, J. (1960). A coefficient of agreement for nominal scales. *Educational and Psychological Measurement, 20(1),* 37–46. https://doi.org/10.1177/001316446002000104

17. Calkins, H., Kuck, K. H., Cappato, R., Brugada, J., Camm, A. J. et al. (2012). 2012 HRS/EHRA/ECAS expert consensus statement on catheter and surgical ablation of atrial fibrillation: Recommendations for patient selection, procedural techniques, patient management and follow-up, definitions, endpoints, and research trial design. *Europace, 14(4),* 528–606. https://doi.org/10.1093/europace/eus027

18. Vogt, F. M., Theysohn, J. M., Michna, D., Hunold, P., Neudorf, U. et al. (2013). Contrast-enhanced time-resolved 4D MRA of congenital heart and vessel anomalies: Image quality and diagnostic value compared with 3D MRA. *European Radiology, 23(9),* 2392–2404. https://doi.org/10.1007/s00330-013-2845-7

19. Sorensen, T. S., Korperich, H., Greil, G. F., Eichhorn, J., Barth, P. et al. (2004). Operator-independent isotropic three-dimensional magnetic resonance imaging for morphology in congenital heart disease: A validation study. *Circulation, 110(2),* 163–169. https://doi.org/10.1161/01.CIR.0000134282.35183.AD

20. Fratz, S., Chung, T., Greil, G. F., Samyn, M. M., Taylor, A. M. et al. (2013). Guidelines and protocols for cardiovascular magnetic resonance in children and adults with congenital heart disease: SCMR expert consensus group on congenital heart disease. *Journal of Cardiovascular Magnetic Resonance, 15(1),* 51. https://doi.org/10.1186/1532-429X-15-51

21. Tomasian, A., Lohan, D. G., Laub, G., Singhal, A., Finn, J. P. et al. (2008). Noncontrast 3D steady state free precession magnetic resonance angiography of the thoracic central veins using nonselective radiofrequency excitation over a large field of view: Initial experience. *Investigative Radiology, 43(5),* 306–313. https://doi.org/10.1097/RLI.0b013e31816be927

22. Hu, P., Stoeck, C. T., Smink, J., Peters, D. C., Ngo, L. et al. (2010). Noncontrast SSFP pulmonary vein magnetic resonance angiography: Impact of off-resonance and flow. *Journal of Magnetic Resonance Imaging, 32(5),* 1255–1261. https://doi.org/10.1002/jmri.22356

23. Gamper, U., Boesiger, P., Kozerke, S. (2008). Compressed sensing in dynamic MRI. *Magnetic Resonance in Medicine, 59(2),* 365–373. https://doi.org/10.1002/(ISSN)1522-2594

24.  Lustig, M., Donoho, D., Pauly, J. M. (2007). Sparse MRI: The application of compressed sensing for rapid MR imaging. *Magnetic Resonance in Medicine, 58(6),* 1182–1195. https://doi.org/10.1002/(ISSN)1522-2594

25.  Porras, D., Kratz, C., Loukas, M., van Doesburg, N. H., Davignon, A. et al. (2003). Superoinferior ventricles with superior left ventricle and inferior right ventricle: A newly recognized form of congenital heart disease. *Pediatric Cardiology, 24(6),* 604–607. https://doi.org/10.1007/s00246-002-0396-9

**Supplementary Material**

*Video 1 (.MP4 file)*

### Clinical case example I (same case as shown in Fig. 3)

Three-dimensional whole heart imaging using nonselective balanced SSFP with compressed SENSE (nsWHcs) in an 11-year-old boy (bodyweight, 20 kg; heart rate, 65/min; propofol sedation) with a single ventricle and total cavopulmonary connection with intracardiac lateral tunnel prior to radiofrequency ablation of ectopic atrial tachycardia. Note the flow-independent homogeneous blood pool signal in all vascular compartments/endoluminal cavities resulting in clear depiction of the fenestration site of the intracardiac lateral tunnel which is crucial for guidance of atrial catheter access.

*Video 2 (.MP4 file)*

### Clinical case example II (same case as shown in Fig. 4)

A 48-year-old male (bodyweight, 82 kg; heart rate 65/min; diazepam sedation) with prior surgical ventricular septal defect (VSD) closure in early childhood presented with progressive pulmonary hypertension and new-onset atrial flutter raising suspicion of residual VSD. CMR imaging identified extracardiac shunting from an aortopulmonary window (luminal diameter 7 mm) located about 25 mm cranial of the left coronary cusp of the aortic valve with continuous systolic-diastolic jet-related flow disturbances. Percutaneous occluder implantation was successfully performed.

*Video 3 (.MP4 file)*

### Clinical case example III (same case as shown in Fig. 5)

A 5-year-old boy (bodyweight, 14 kg; heart rate, 85/min; propofol sedation) with a single ventricle (hypoplastic right heart syndrome) after bilateral bidirectional Glenn procedure was scheduled for radiofrequency ablation of an accessory pathway prior to finalizing staged palliative surgery leading to total cavopulmonary connection. Preinterventional CMR imaging identified "supero-inferior ventricle" anatomy with tricuspid annulus and contractile, rudimentary right-ventricular cavity [25]. On subsequent invasive electrophysiological testing, atriofascicular pathway tachycardia ("Mahaim") was identified and successful radiofrequency ablation performed at the lateral tricuspid valve annulus and neighboring myocardium of the rudimentary right ventricle.